Atmospheric Research 169 (2016) 86–95

Contents lists available at ScienceDirect

Atmospheric Research

journal homepage: www.elsevier.com/locate/atmos

Evolution of particulate sulfate and nitrate along the Asian dust pathway: Secondary transformation and primary pollutants via long-range transport

Qiongzhen Wang [a,d,e], Guoshun Zhuang [a,*], Kan Huang [b,*], Tingna Liu [a], Yanfen Lin [c], Congrui Deng [a], Qingyan Fu [c], Joshua S. Fu [b], Jiakuan Chen [d], Wenjie Zhang [f], Mijiti Yiming [g]

[a] Department of Environmental Science and Engineering, Center for Atmospheric Chemistry Study, Fudan University, Shanghai, 200433, PR China
[b] Department of Civil and Environmental Engineering, University of Tennessee, Knoxville, TN 37996, USA
[c] Shanghai Environmental Monitoring Center, Shanghai, 200030, China
[d] School of Life Sciences, Fudan University, Shanghai, 200433, China
[e] Zhejiang Environmental Science & Design Institute, Hangzhou, Zhejiang, 310007, China
[f] Chinese Research Academy of Environmental Sciences, Beijing 100012, China
[g] Hetian Environmental Monitoring Center, Hetian, 848000, China

ARTICLE INFO

Article history:
Received 29 May 2015
Received in revised form 3 September 2015
Accepted 16 September 2015
Available online 30 September 2015

Key words:
Sulfate
Nitrate
Source
Formation mechanism
Long-range/regional transport

ABSTRACT

Both $PM_{2.5}$ and TSP over Yulin, a rural site near the Asian dust source region, were collected from 2007 to 2009. Characteristics, sources, and formation mechanisms of sulfate and nitrate were investigated. SO_4^{2-} displayed a distinct seasonal variation with the highest average concentration observed in summer when SO_4^{2-} accounted for an average of 14.1% and 13.7% of the $PM_{2.5}$ and PM_{coarse} mass concentrations, respectively. Ambient temperature and relative humidity were two important factors influencing the formation processes of SO_4^{2-} and NO_3^-. In summer, the high concentrations of SO_4^{2-} in $PM_{2.5}$ were probably from the gas phase oxidation of SO_2, while the low concentrations of NO_3^- in $PM_{2.5}$ were attributed to the high temperature that was not favorable for the formation of NH_4NO_3. In spring, autumn, and winter, SO_4^{2-} and NO_3^- were significantly enhanced in those days with high relative humidity, implying that in-cloud/aqueous processing dominated the formations of SO_4^{2-} and NO_3^-. Different from $PM_{2.5}$ in which NH_4^+ acted as the dominant neutralizer for acids, alkaline species such as Ca^{2+} and Mg^{2+} played an important role in the formation of sulfate and nitrate salts in coarse particles throughout the whole year. During the dust event days, SO_4^{2-} in coarse particles significantly increased, while black carbon and NO_3^- largely decreased, suggesting that the primary mineral dust could be one of the major sources of SO_4^{2-}. By comparing the mass ratio of SO_4^{2-}/3/S in the dust aerosols of Yulin with different dust source regions (i.e., Taklimakan Desert and Gobi Desert) and the application of air mass backward trajectory analysis, it was found the long-range transported dust from the Taklimakan Desert, which was rich in primary sulfate due to its paleo-ocean characteristics, was a non-negligible source of SO_4^{2-} over Yulin. In spring and winter, the prevailing northerlies and northwesterlies promoted chemical interaction between alkaline mineral dust and acid gaseous precursors from local and/or regional emissions. While in summer, regional transport facilitated by the southerlies and southeasterlies may contribute to the high secondary aerosol concentrations over Yulin. This study demonstrated that a considerable portion of aerosol over a Chinese rural area could be derived from complex chemical reactions via long-range/regional transport.

1. Introduction

Asian dust and its transport have great impacts on regional air quality (e.g., Fu et al., 2008; Zhao et al., 2011) as it carries not only mineral aerosols but also pollution matter to the atmosphere over the downwind regions. During the transport, mineral aerosols can mix and interact with anthropogenic pollutants, leading to a significant increase of pollution matters, such as sulfate and nitrate (Manktelow et al., 2010; Usher et al., 2002; Zhang et al., 2000). The formation of sulfate and nitrate on mineral particles influences the hydrophilicity of the particles (Shi et al., 2008), which in turn can impact the further chemical reactions on the particles. The modification of dust aerosol during the transport can cause high uncertainties in evaluating its environmental effects.

Sulfate is of great concern for its effect on climate change (IPCC, 2007), and its role in atmospheric chemical and physical processes (Sipila et al., 2010; Yue et al., 2010). Nitrate is now attracting more and more attention, as NO_X emission has been increasing across China over the past decade (Guinot et al., 2007; Streets et al., 2003; Zhang et al., 2007). As both sulfate and nitrate are two major water-soluble ions in aerosols, the high emissions of SO_2 and NO_X, their transformations to

* Corresponding authors.
E-mail addresses: gzhuang@fudan.edu.cn (G. Zhuang), khuang7@utk.edu (K. Huang).

http://dx.doi.org/10.1016/j.atmosres.2015.09.013
0169-8095/

sulfate and nitrate, and their long/medium-range transport would have significant impact on the air quality of the downwind regions.

China is now a hot spot region for air pollution and global climate change studies (Chang et al., 2010; Morino et al., 2011). Intensive studies were designed to investigate the sources and formation mechanisms of particulate sulfate and nitrate over China (e.g., Guo et al., 2010a; Xiao et al., 2009; Yao et al., 2002). However, most studies focused on big urban cities, while relatively few studies were conducted for remote areas nearby the dust sources, where the interaction between the natural mineral dust and anthropogenic emissions were most active. Yulin, the sampling site in this study, is located at the northern edge of the Chinese Loess Plateau and on the transport pathway of Asian dust from northern and northwestern China to the North Pacific (Zhang et al., 2008). It is also in the depositional region of the dust from both the Taklimakan Desert (Liu et al., 1994) and Gobi Desert (Sun et al., 2001). In addition, Yulin is surrounded by a number of big coal mines with intensive industrial activities. In this regard, Yulin could be treated as a good representative site for investigating aerosols from complex sources. In this study, a multi-year sampling of aerosol was conducted at Yulin, and the characteristics and sources of sulfate and nitrate were probed. Specifically, different formation mechanisms of secondary aerosol were studies on a seasonal basis.

2. Methods

2.1. Study site and field sampling

Both $PM_{2.5}$ (particle size smaller than 2.5 μm) and TSP (total suspended particles) were collected in Yulin (YL), Shaanxi province of China, and its location is shown in Fig. 1. YL is the northernmost prefecture-level city of Shaanxi province and lies in the transition zone between the Loess Plateau and deserts. As shown in Fig. 1, to the north and northwest of the city it is the Ordos Desert (also known as Mu Us Desert) of Inner Mongolia. YL is characterized of a continental, monsoon-influenced semi-arid climate. The definition of the four seasons in this study is from March to May for spring, June to August for summer, September to November for autumn, and December to February for winter, respectively, with each season encompassing the entirety of the included months. In winter, it is very cold with rather long durations, while in summer, it is hot and somewhat humid. Desertification due to wind erosion has been severe in this region. Aerosol samples were collected from 2007 to 2009 to study the characteristics of mineral and pollution aerosol over the areas nearby dust sources. The samplers were set up about 10 m above the ground. Aerosol sampling in 2007 was conducted from March 20 to April 22 to monitor dust events, while in 2008–2009, it was conducted in four separated periods, i.e., March 21, 2008, to April 18, 2008; July 21, 2008, to August 22, 2008; October 15, 2008, to November 15, 2008; and January 15, 2009, to February 15, 2009, to represent the four seasons of spring, summer, autumn, and winter, respectively. Aerosol samples (the sampling generally lasted for 24 h) were collected on Whatman 41 filters (Whatman Inc., Maidstone, UK) by medium-volume samplers (model: $(TSP/PM_{10}/PM_{2.5})$-2, flow rate: 77.59 L min^{-1}). All the samples were put in polyethylene plastic bags immediately after sampling and then stored in a refrigerator before the weighing and chemical analysis. All the filters were weighed before and after sampling with an analytical balance (Sartorius BT 25 s, reading precision: 10 μg) after stabilizing under constant temperature (20 ± 1 °C) and humidity (40 ± 2 %) for over 48 h. All the procedures were strictly quality controlled to avoid any possible contamination of the samples.

2.2. Chemical analysis

2.2.1. Ion analysis

One-fourth of each sample filter and blank filters were extracted ultrasonically by 10 ml deionized water (18 MΩ cm^{-1}). SO_4^{2-}, NO_3^-, Cl^-, NH_4^+, Na^+, K^+, Ca^{2+}, and Mg^{2+} were analyzed by an Ion Chromatography (Dionex ICS 3000, USA), which consists of a separation column (Dionex Ionpac AS 11 for anion, Dionex IonPac CS 12A for cation), a guard column (Dionex Ionpac AG 11 for anion, Dionex IonPac AG 12A for cation), a self-regenerating suppressed conductivity detector (Dionex Ionpac ED50), and a gradient pump (Dionex Ionpac GP50). The detailed procedures were given elsewhere (Yuan et al., 2003).

2.2.2. Element analysis

Half of each sample filter and blank filters was digested at 170 °C for 4 h in a high-pressure Teflon digestion vessel with 3 ml concentrated HNO_3, 1 ml concentrated $HClO_4$, and 1 ml concentrated HF. After cooling, the solutions were dried and then diluted to 10 ml with deionized water (18 MΩ cm^{-1}). Eighteen elements including Al, Fe, Mn, Mg, Ti, Na, Sr, Ca, Co, Cr, Ni, Cu, Pb, Zn, Cd, V, S, and As were determined by an inductively coupled plasma atomic emission spectroscopy (ICP-AES, Model: ULTIMA, JOBIN-YVON Company, France). The detailed analytical procedures were given elsewhere (Zhuang et al., 2001).

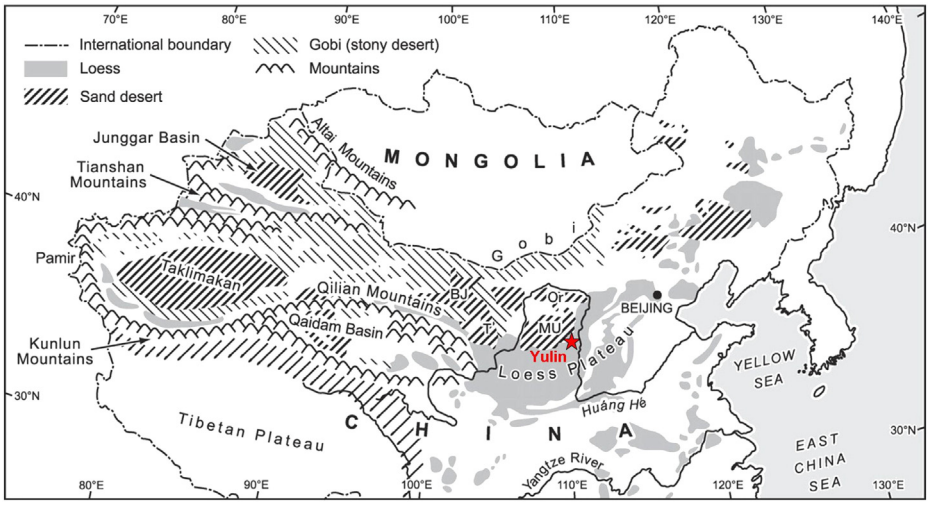

Fig. 1. The location of the sampling site (Yulin, Shaanxi province, China) indicated by the red star. The background map is modified based on the chapter "The Loess Plateau Geography 5" from WordPress.com (https://geog5loessplateau.wordpress.com/).

2.2.3. Black carbon analysis

Black carbon (BC) in each sample and blank filters was measured by a Smoke Stain Reflectometer (Model M43D, Diffusion Systems Ltd., London, UK). The concentrations are determined based on the amount of reflected light absorbed by the aerosol samples on each filter and calibrated using BC gravimetric standards.

2.3. Meteorological parameters, acid gases, and modeling of air mass trajectories

The meteorological data, including ambient temperature, relative humidity, wind speed, wind direction, etc., were obtained from NOAA's National Climatic Data Center (NCDC), available on a 3-h basis from 2:00 to 23:00 every day. Three-day air mass back trajectories initiated at 500 m from the Yulin measurement site were calculated using the HYSPLIT model (R. Draxler and G. Rolph, HYSPLIT (HYbrid Single-Particle Lagrangian Integrated Trajectory) Model, 2003, http://ready.arl.noaa.gov/HYSPLIT.php) and driven by the Global Data Assimilation System (GDAS, 1° × 1° resolution) data set.

The bimonthly average concentrations of SO_2 and NO_2 were documented in the periodic reports from Shaanxi Provincial Environmental Protection Department (Shaanxi EPD, 2007–2009).

3. Results and discussion

3.1. Seasonal variations of aerosols and water-soluble inorganic ions

3.1.1. Aerosol concentrations

Fig. 2f shows the variations of the daily $PM_{2.5}$ and TSP concentrations during each sampling period in the spring 2007 to winter 2008. It is clearly shown that more extreme events (i.e., high aerosol concentrations) occurred in spring and winter. However, as indicated by the average concentrations of $PM_{2.5}$ in four seasons of 2008 in Table 1, $PM_{2.5}$ concentrations in summer and autumn were slightly higher than those in spring and winter, which was in contrast to most studies. The monthly aerosol optical depth (AOD) values at the Yulin AERONET (AErosol RObotic NETwork, http://aeronet.gsfc.nasa.gov/) site also showed highest values in summer (Fig. S1), which was consistent with this study. Although YL is a rural site, the average $PM_{2.5}$

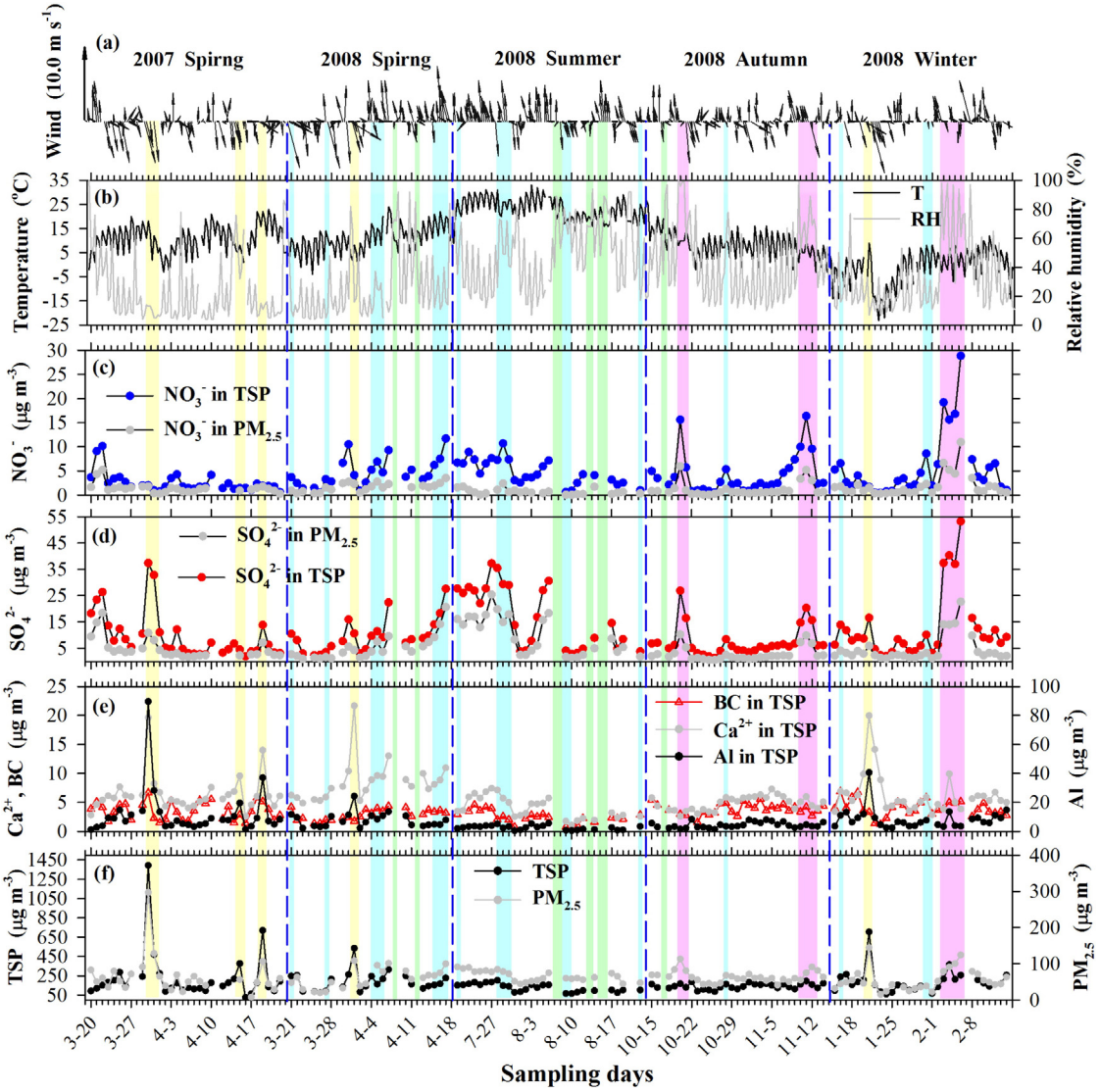

Fig. 2. Time series of (a) three hourly wind vectors and (b) ambient temperature and relative humidity. Daily variations of (c) NO_3^- in $PM_{2.5}$ and TSP; (d) SO_4^{2-} in $PM_{2.5}$ and TSP; (e) Ca^{2+}, BC, and Al in TSP; and (f) the mass concentrations of $PM_{2.5}$ and TSP (note that $PM_{2.5}$ and TSP use different *Y*-axis) during the whole sampling period, which is separated by the blue dashed lines on the seasonal basis. The yellow, green, cyan, and pink bars represent dust, rainy, cloudy, and foggy days, respectively.

Table 1
Monthly average concentrations of particulate mass concentrations, black carbon, and the inorganic ions ($\mu g m^{-3}$) in $PM_{2.5}$ and PM_{coarse} and their $PM_{2.5}$/TSP ratios. PM_{coarse} represents the coarse mode mass of particulate matters calculated based on the difference between TSP and $PM_{2.5}$.

	Spring			Summer			Autumn			Winter		
	$PM_{2.5}$	PM_{coarse}	$PM_{2.5}$/TSP	$PM_{2.5}$	PM_{coarse}	$PM_{2.5}$/TSP	$PM_{2.5}$	PM_{coarse}	$PM_{2.5}$/TSP	$PM_{2.5}$	PM_{coarse}	$PM_{2.5}$/TSP
PM	59.7	129.7	0.32	66.1	61.0	0.56	62.4	78.7	0.44	56.4	136.6	0.29
BC	1.5	1.4	0.53	1.4	1.0	0.60	2.2	1.7	0.56	2.0	2.0	0.51
Cl^-	0.8	0.9	0.46	0.3	0.3	0.51	0.3	0.8	0.32	0.6	1.4	0.32
NO_3^-	1.7	3.3	0.36	0.7	4.0	0.15	1.1	2.9	0.28	1.9	3.8	0.33
SO_4^{2-}	5.2	4.6	0.53	10.1	7.2	0.57	2.7	4.7	0.37	4.6	8.0	0.37
NH_4^+	2.8	1.2	0.73	4.1	2.6	0.61	1.6	1.6	0.49	2.5	2.3	0.52
Na^+	0.5	0.6	0.43	0.1	0.1	0.52	0.2	0.3	0.38	0.3	1.1	0.22
K^+	0.3	0.4	0.41	0.1	0.1	0.55	0.1	0.2	0.39	0.3	0.5	0.40
Mg^{2+}	0.3	0.2	0.56	0.1	0.1	0.39	0.1	0.2	0.36	0.1	0.2	0.35
Ca^{2+}	3.4	5.1	0.40	0.7	3.4	0.16	1.2	3.7	0.24	1.2	4.3	0.23

concentrations were ~60–90% higher than the Chinese annual standard of 35 $\mu g m^{-3}$ throughout all seasons. In summer, daily $PM_{2.5}$ concentrations exceeded the Chinese daily standard of 75 $\mu g m^{-3}$ in more than one third of the 26 non-precipitation sampling days. Compared to $PM_{2.5}$, the concentrations of coarse particles (PM_{coarse}), i.e., the difference between the measured concentrations of TSP and $PM_{2.5}$ (TSP-$PM_{2.5}$), presented a distinct seasonal variation with the sequence of winter/spring > summer/autumn (Table 1). As YL is nearby the dust source regions as introduced in Section 2.1, the aerosols there should be highly impacted by mineral dust. Fig. 2a shows the winds in spring and winter frequently came from the west, northwest, and the north with relatively higher wind speeds (4.3–5.2 m s^{-1}) than the other seasons (3.8–4.3 m s^{-1}). Under this synoptic condition, mineral dust from those dust source regions (Fig. 1) could be brought to YL. While in summer, the prevailing winds dominantly blew from the south and the southeast. YL is located at the north edge of the Chinese Loess Plateau; the regions to its south and southeast were characterized of high emissions of anthropogenic pollutants such as SO_2 and NOx (Streets and Waldhoff, 2000). Hence, regional transport from those relatively polluted regions to YL should be ubiquitous via the southerlies and southeasterlies. This may partly explain why the mass ratio of $PM_{2.5}$/TSP was much higher in summer (56%) than that in spring, autumn, and winter (29–44%), as pollution aerosols, unlike mineral dust, accumulated preferentially in $PM_{2.5}$ than in PM_{coarse}.

3.1.2. Water-soluble inorganic ions

As shown in Table 1, SO_4^{2-} was the most abundant species among all ions in four seasons. SO_4^{2-} displayed a pronounced seasonal variation in a descending manner of summer > spring/winter > autumn in $PM_{2.5}$. While in PM_{coarse}, it followed the sequence of winter/summer > spring/autumn. Apparently, both coarse and fine modes of particulate SO_4^{2-} were significantly enhanced in summer (Fig. 2d and S2c). In summer, the highest daily SO_4^{2-} concentration could reach up to 25.4 $\mu g m^{-3}$ in $PM_{2.5}$ and 37.3 $\mu g m^{-3}$ in TSP. The SO_4^{2-} concentration in $PM_{2.5}$ over YL in summer was even higher than that of a Chinese megacity, Shanghai (Wang et al., 2006), although the emission rate of SO_2, the precursor of SO_4^{2-}, was much less intensive in YL (Zhang et al., 2009). It is calculated that SOR (sulfur oxidation ratio, SOR = $SO_4^{2-}/(SO_2 + SO_4^{2-})$) in YL in summer reached about 0.29, much higher than that of 0.05 in Shanghai in summer (Wang et al., 2006). As a coastal city, Shanghai is dominated by the southerlies and southeasterlies from the ocean in summer. Sea breeze has a cleansing effect and could dilute the concentrations of particles; thus, the concentration of sulfate observed in Shanghai was low and resulted in a low SOR. Different from Shanghai, Yulin is an inland city without any influences from sea breezes. Oppositely, the prevailing southeasterlies in Yulin in summer (Fig. 2a) could bring in more pollutants as more cities are located to the south of Yulin. In this regard, the higher SOR in summer over Yulin is expected. The average SO_4^{2-} concentrations in other seasons were much lower than that in summer (Table 1). However, extremely high SO_4^{2-} concentrations could still be observed with daily concentrations reaching up to over 20 $\mu g m^{-3}$ in $PM_{2.5}$ and 50 $\mu g m^{-3}$ in TSP. Those SO_4^{2-} peaks in autumn and winter were mostly observed in foggy/cloudy days (Fig. 2), when the oxidation of SO_2 could be significantly promoted due to the aqueous processing (Seinfeld and Pandis, 2006). In those days without dust events in spring, SO_4^{2-} increased along with the increase of relative humidity (RH), indicating that RH played an important role in the formation of particulate SO_4^{2-} (See more details in Section 3.3). While during the dust events, SO_4^{2-} was also observed to be greatly enhanced, particularly in PM_{coarse} (Fig. S2c), suggesting part of SO_4^{2-} could be from the crustal source, which will be explicitly discussed in Section 3.4.

NO_3^- was less than 50% of SO_4^{2-} in $PM_{2.5}$ in four seasons, and its average concentration followed as winter > spring > autumn > summer. In winter, the average NO_3^- concentration in $PM_{2.5}$ was ~170% higher than that in summer. More NOx emissions due to domestic heating in the cold seasons in Northern China should be the major cause of this seasonal variation of NO_3^- concentrations. In addition, the lower ambient temperature in the cold seasons favored the accumulation of nitrate (e.g., NH_4NO_3) in particulate phase. In PM_{coarse}, the average concentrations of NO_3^- were ~50–70% of that of SO_4^{2-}. Compared to the NO_3^- concentrations of 2.6–9.1 $\mu g m^{-3}$ in Shanghai (Wang et al., 2006) and that of 9.6–20.6 $\mu g m^{-3}$ in Xi'an (Zhang et al., 2011), the seasonal $PM_{2.5}$ NO_3^- concentrations of 0.7–1.9 $\mu g m^{-3}$ in YL were much lower. However, compared to a site (Tazhong) located in the center of Taklimakan Desert with NO_3^- concentrations less than 0.6 $\mu g m^{-3}$ in $PM_{2.5}$ and 2.0 $\mu g m^{-3}$ in TSP (unpublished data), NO_3^- over YL was considerably higher, implying there were moderate anthropogenic activities in and around YL. Similar to the temporal variation of SO_4^{2-}, high peaks of NO_3^- were also mostly observed in the circumstance of foggy and cloudy weather with maximum daily concentration reaching up to 11 $\mu g m^{-3}$ in $PM_{2.5}$ and 28 $\mu g m^{-3}$ in TSP, suggesting an important role of aqueous processing in the formation of NO_3^- during those heavily polluted days. It is noted that the seasonal $PM_{2.5}$/TSP ratio for NO_3^- ranged from 0.15 to 0.36, while for SO_4^{2-} ranged from 0.37 to 0.57 (Table 1), indicating that NO_3^-, unlike SO_4^{2-}, accumulated more in coarse particles than in fine particles. This indicated that the formation processes of NO_3^- and SO_4^{2-} were quite different, which will be further discussed in Section 3.3.

NH_4^+ ranked as the most abundant species among all cations in $PM_{2.5}$ except in spring, while in PM_{coarse}, it was only inferior to Ca^{2+} (Table 1). NH_4^+ displayed a seasonal variation of summer > spring > winter > autumn in $PM_{2.5}$, while it followed as summer > winter > autumn > spring in PM_{coarse}. In average, NH_4^+ accounted for 5.7% (in the range of 1.0–12.7%) of $PM_{2.5}$ and 4.5% (in the range of 0.9–8.4%) in PM_{coarse} in summer, higher than those in the other seasons. The high concentrations of NH_4^+ in summer should be attributed to the southern and southeastern winds that would bring in more polluted air masses to YL than in the other seasons (Fig. 2a). This partly explained why SO_4^{2-} showed the highest concentration in summer as mentioned above.

Ca^{2+}, Mg^{2+}, and Na^{+} were mostly characterized of crustal origin and showed the highest concentrations in spring when dust events frequently occurred. As a comparison, the concentrations of these ions were relatively low in summer as much less dust events occurred. In addition to NH_3, crustal components, such as $CaCO_3$ and $MgCO_3$ also played an important role in the formation of sulfate and nitrate (see below Section 3.3.1), especially in the coarse mode of particles (Li et al., 2006; Lin, et al., 2014; Takahashi et al., 2008).

Fig. 3 shows the mass contributions of the major components to $PM_{2.5}$ and PM_{coarse} in four seasons. The concentration of minerals was calculated as Minerals = 1.16 (1.9Al + 2.15Si + 1.14Ca + 1.47Ti + 2.09Fe) (Malm et al., 1994). As Si was not directly measured in this study, it was estimated as Si = 3.43Al, based on the crustal abundance of Al and Si in earth (Lida, 2006). The difference between the total aerosol mass and the sum of inorganic ions, minerals, and BC was labeled as "Others" in Fig. 3, of which should be primarily carbonaceous matters that were unmeasured in this study, water content associated with the hygroscopic aerosol components, and other species that could not be detected with the available instrumentation. As expected, minerals accounted for a majority of PM_{coarse} in all seasons because YL is located at the north edge of the Chinese Loess Plateau where mineral dusts are abundant. The ratios of minerals/$PM_{2.5}$ and minerals/PM_{coarse} were lowest in summer. In particular, the average ratio of minerals/$PM_{2.5}$ was as low as 11.3% in summer, indicating the dominance of anthropogenic sources contributing to $PM_{2.5}$ formation in summer. In summer, the average mass ratio of SO_4^{2-} reached 14.1% in $PM_{2.5}$ and 13.7% in PM_{coarse}, while it was 4.1–8.0% in $PM_{2.5}$ and 3.6–6.5% in PM_{coarse} in the other seasons. As for NO_3^-, the average ratio of $NO_3^-/PM_{2.5}$ in summer was the lowest among the four seasons, while the ratio of NO_3^-/PM_{coarse} was the highest, again showing that NO_3^- was more favorably formed in coarse particles in summer. On average, the ratio of the sum of SO_4^{2-}, NO_3^-, and NH_4^+ (SNA) in $PM_{2.5}$ was 15.4%, 8.2%, and 14.9% in spring, autumn, and winter, and in PM_{coarse} was 7.3%, 12.7%, and 11.3%, respectively, while those ratios increased to 20.9% and 25.8% in $PM_{2.5}$ and PM_{coarse}, respectively, in summer.

3.2. Acid gaseous precursors

SO_4^{2-} and NO_3^- in aerosols are mostly related to the transformation of their acid precursors, i.e., SO_2 and NOx. Fig. 4 shows the bimonthly average concentrations of SO_2 and NO_2 in YL from November 2007 to February 2009. SO_2 and NO_2 in Yan'an and Xi'an, another two cities nearby YL, are also shown to reveal the regional air pollution level. At these three sites, SO_2 was highest in November–February among the whole year, i.e., in later autumn and winter, with high concentrations of 68–117 μg m^{-3} in YL, 56–78 μg m^{-3} in Xi'an, and 126–157 μg m^{-3} in Yan'an, respectively. The concentration level in this region mostly exceeded the Chinese annual standard of 60 μg m^{-3}, indicating a high regional emission of SO_2 during this period. The average SO_2 concentration was lowest in May–August (except in Yan'an), i.e., in later spring and summer due to the lower emissions and favorable meteorological conditions. The average SO_2 concentration in July–August of 2008 was 77% lower than that in January–February of 2009 in YL, while SO_4^{2-} in $PM_{2.5}$ in summer was ~120% higher than that in winter. This suggested the formation efficiency from SO_2 to SO_4^{2-} was significantly enhanced in summer, compared to that in winter. During the domestic heating period (generally from November 15 to March 15), the concentrations of SO_2 increased greatly at all three cities. Enhanced fossil fuel combustion from domestic heating was the major contributor to SO_2 emissions in the cold season (Lu et al., 2010). Biomass burning was another potential source of SO_2 (Streets and Waldhoff, 2000). During the harvest time in fall, burning of crop residuals, such as corn and wheat residuals, could

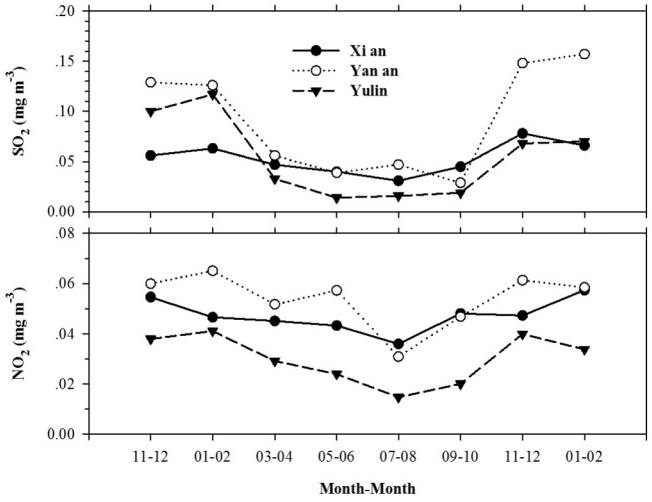

Fig. 4. Bimonthly average concentrations of SO_2 and NO_2 over Yulin, Yan'an, and Xi'an from November 2007 to February 2009.

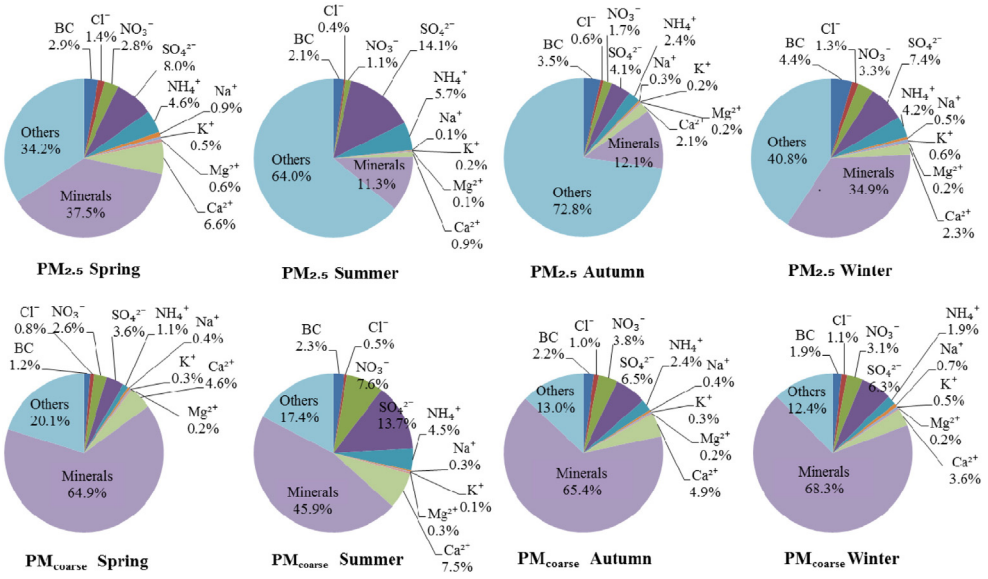

Fig. 3. Mass contributions of chemical compositions to $PM_{2.5}$ and PM_{coarse} in four seasons. PM_{coarse} represents the coarse mode mass of particulate matters calculated based on the difference between TSP and $PM_{2.5}$.

be a significant source of SO_2. In addition, biofuel that was burned for rural residential cooking and heating was another source of SO_2. However, compared to fossil fuel burning, the emission from biomass burning was not significant on a long-time scale (Streets et al., 2003).

Similar to SO_2, the bimonthly variation of NO_2 at these three sites also showed highest concentrations in November–February and lowest concentrations in July–August. The average NO_2 concentration in November–February reached 34–41 μg m^{-3} in YL, Yan'an, and Xi'an, suggesting the enhanced fossil fuel combustion for winter heating on the regional scale. In YL, the average NO_2 concentration in July–August of 2008 was 44% of that in January–February of 2009, while the average TSP NO_3^- concentration in summer was ~80% of that in winter, implying that the formation efficiency from NO_X to NO_3^- was also greater in summer than in winter, as was the case for SO_2.

3.3. Seasonal formation pathways of sulfate and nitrate

3.3.1. Summer

Table 2 lists the correlation coefficients between SO_4^{2-} and NO_3^-, and the five measured cations, i.e., Na^+, NH_4^+, K^+, Mg^{2+}, and Ca^{2+}. In $PM_{2.5}$, SO_4^{2-}, and NO_3^- were highly correlated to NH_4^+ in all seasons except NO_3^- in summer. NH_4^+ was the most abundant cation in $PM_{2.5}$ except in spring (Table 1). Hence, NH_3 acted as the major alkaline species for the neutralization of SO_4^{2-} and NO_3^- in $PM_{2.5}$ over YL. Fig. 5a–d shows the relationship between NH_4^+ and SO_4^{2-}, NO_3^-, and the sum of SO_4^{2-} and NO_3^- in $PM_{2.5}$, respectively. All units are in equivalent concentrations (μeq m^{-3}), and linear regression equations are fitted for NH_4^+ and $[SO_4^{2-} + NO_3^-]$ in the figure. In summer, almost all SO_4^{2-} and NO_3^- in $PM_{2.5}$ had been completely neutralized by NH_3, as the linear regression slope of $[NH_4^+]/[SO_4^{2-} + NO_3^-]$ was slightly higher than unity (Fig. 5b). Compared to those megacity sites of Beijing, Shanghai, and Guangzhou (Pathak et al., 2009; Yao et al., 2002), YL was in a relatively ammonia-rich environment as it is located in the northern agricultural region mainly for planting wheat, soy bean and corn. Hence, SO_4^{2-} and NO_3^- in $PM_{2.5}$ mainly existed in the forms of $(NH_4)_2SO_4$ and NH_4NO_3. In addition, the prevailing southern and southeastern winds in summer could bring considerable pollutants from southerly polluted areas to YL, providing favorable conditions for the gas-to-particle transformation of SO_2 and NOx to SO_4^{2-} and NO_3^- and their further neutralization into the ammonium salts.

Particulate SO_4^{2-} usually forms via pathways such as the oxidation of SO_2 through gas phase reaction, in-cloud/aqueous processing, and heterogeneous reaction on pre-existing particles. The reaction of SO_2 with OH radical is dominant for the production of SO_4^{2-} in the gas phase. The aqueous-phase processing due to high humidity could accelerate the transformation of SO_2 and NOx to acids via the oxidation pathways such as H_2O_2 and O_3 oxidation and metal catalysis (e.g., Fe^{3+} and Mn^{2+}). The dominance of in-cloud/aqueous processing over the gas phase reaction has been observed in various regions of China (Guo et al., 2010b; Yao et al., 2002). However, it was also shown that the gas phase oxidation could account for the formation of SO_4^{2-} in submicron particles over Guangzhou (Xiao et al., 2009), a coastal city with high relative humidity. In this study, whether the gas phase or the in-cloud/aqueous processing was dominant for the formation of SO_4^{2-} could not be quantitatively differentiated. However, we tend to believe that the gas phase reaction should be responsible for the majority of fine mode SO_4^{2-} production in summer. First, high SO_4^{2-} concentrations in $PM_{2.5}$ mostly appeared in sunny days with low relative humidity (daily RH < 50%, and sometimes even lower than 30%, Fig. 2). For instance, SO_4^{2-} in $PM_{2.5}$ reached 13.0–25.4 μg m^{-3} on July 22–27, 2008, with daily RH of 26–46%, and 15.8–18.3 μg m^{-3} on August 5–6, 2008, with daily RH of 31–38%. In comparison, on August 10–14 and 17, when the daily RH was higher at 54–70%, daily $PM_{2.5}$ SO_4^{2-} was only 1.4–8.6 μg m^{-3}. Therefore, we believed that the role of in-cloud/aqueous processing in secondary aerosol formation affecting Yulin was not necessarily the dominant route.

Second, as shown in Fig. 6a (square scatters), the concentration of SO_4^{2-} did not present an increasing trend along with the increase of RH, which was an important factor for in-cloud/aqueous processing. Third, the gas phase reactions of SO_2 are initiated by reaction with OH radical, which is related to the photolysis of ozone in the atmosphere. The high ozone concentration in summer due to strong solar radiation could result in considerable production of OH radicals, leading to a high reaction rate of SO_2 in the gas phase (Calvert and Su, 1978). In a word, the high concentration of SO_4^{2-} observed in summer should be mainly dominated by the gas phase oxidation of SO_2.

NO_3^- did not show significant correlation with NH_4^+ in $PM_{2.5}$ in summer (Table 2 and blue triangles in Fig. 5b). It has been clear that the formation of nitrate in the atmosphere has different pathways in daytime and nighttime. During daytime, HNO_3 can be produced via the gas phase oxidation reaction of $OH\cdot + NO_2 + M = HNO_3 + M$. While in the nighttime, NO_2 reacts with O_3 to form the NO_3 radical and then further reacts with NO_2 to form N_2O_5. N_2O_5 is finally hydrolyzed to produce NO_3^- (Seinfeld and Pandis, 2006). Hence, the oxidation of nitrogen oxides should be favored in summer due to relative strong production of OH radical and O_3. However, NO_3^- was lowest in summer compared to the other seasons, and this should be mainly attributed to the thermal decomposition of ammonium nitrate under high ambient temperature. Furthermore, in a system that contains both H_2SO_4 and HNO_3, NH_3 preferentially neutralizes H_2SO_4 and then the excess NH_3 reacts with HNO_3. Therefore, the low concentration of NO_3^- in $PM_{2.5}$ in summer can also be attributed to the high sulfate concentrations. Our result is consistent with the study by Kong et al. (2014) that found the mass fraction of sulfate was strongly negatively correlated with nitrate at three Chinese urban sites.

Compared to $PM_{2.5}$, the slope of the regression equation between NH_4^+ and $[SO_4^{2-} + NO_3^-]$ was much lower for PM_{coarse} (0.65) than for $PM_{2.5}$ (1.02) (Fig. 5f), suggesting that NH_3 was not enough for fully neutralizing SO_4^{2-} and NO_3^-. In contrast, by adding Ca^{2+} and Mg^{2+}, the linear regression between $[NH_4^+ + Ca^{2+} + Mg^{2+}]$ and $[SO_4^{2-} + NO_3^-]$ showed a slope of 1.26 with high correlation coefficient of 0.90 (Fig. 5f). In summer, Ca^{2+} in PM_{coarse} showed a higher abundance than NH_4^+ (Table 1). The results above revealed that in addition to NH_3, the crustal species (e.g., $CaCO_3$, $MgCO_3$, etc.) played an important role in the formation of coarse mode SO_4^{2-} and NO_3^-. As indicated in Table 1, NO_3^- in PM_{coarse} accounted for ~85% of the total nitrate in TSP while accounting for only ~43% of SO_4^{2-}, suggesting that the heterogeneous reactions on alkaline minerals was more evident for the formation of NO_3^- than SO_4^{2-} in coarse particles.

3.3.2. Other seasons (spring/autumn/winter)

As similar to summer, SO_4^{2-} and NO_3^- in $PM_{2.5}$ during spring, autumn, and winter were also highly correlated to NH_4^+ and the regression slopes of NH_4^+ vs. $[SO_4^{2-} + NO_3^-]$ were higher than unity (Fig. 5a and 5c–d), suggesting YL was in the ammonia-rich environment throughout the whole year. Different from $PM_{2.5}$, the slopes of NH_4^+

Table 2
The Pearson correlation coefficients of SO_4^{2-} and NO_3^- and the five cations in $PM_{2.5}$ and PM_{coarse}. Bold numbers represent the correlations are significant at the 0.05 level.

		Spring		Summer		Autumn		Winter	
		NO_3^-	SO_4^{2-}	NO_3^-	SO_4^{2-}	NO_3^-	SO_4^{2-}	NO_3^-	SO_4^{2-}
$PM_{2.5}$	Na^+	0.09	0.14	0.38	**0.69**	0.30	0.40	−0.02	0.06
	NH_4^+	**0.74**	**0.96**	0.38	**1.00**	**0.88**	**0.95**	**0.96**	**0.97**
	K^+	**0.70**	0.45	0.31	**0.91**	**0.67**	**0.68**	0.38	0.38
	Mg^{2+}	0.35	0.05	**0.68**	**0.67**	0.49	0.43	0.07	0.14
	Ca^{2+}	0.26	0.16	0.23	**0.82**	0.46	0.35	−0.21	−0.21
PM_{coarse}	Na^+	0.03	0.48	**0.62**	**0.63**	0.20	0.01	0.20	0.01
	NH_4^+	**0.69**	**0.64**	**0.54**	**0.90**	**0.77**	**0.90**	**0.86**	**0.83**
	K^+	0.42	0.42	0.13	0.43	**0.77**	**0.68**	0.47	0.41
	Mg^{2+}	**0.49**	**0.55**	0.49	**0.56**	0.23	0.14	**0.73**	**0.80**
	Ca^{2+}	**0.73**	**0.50**	**0.83**	**0.75**	0.12	0.05	**0.53**	**0.63**

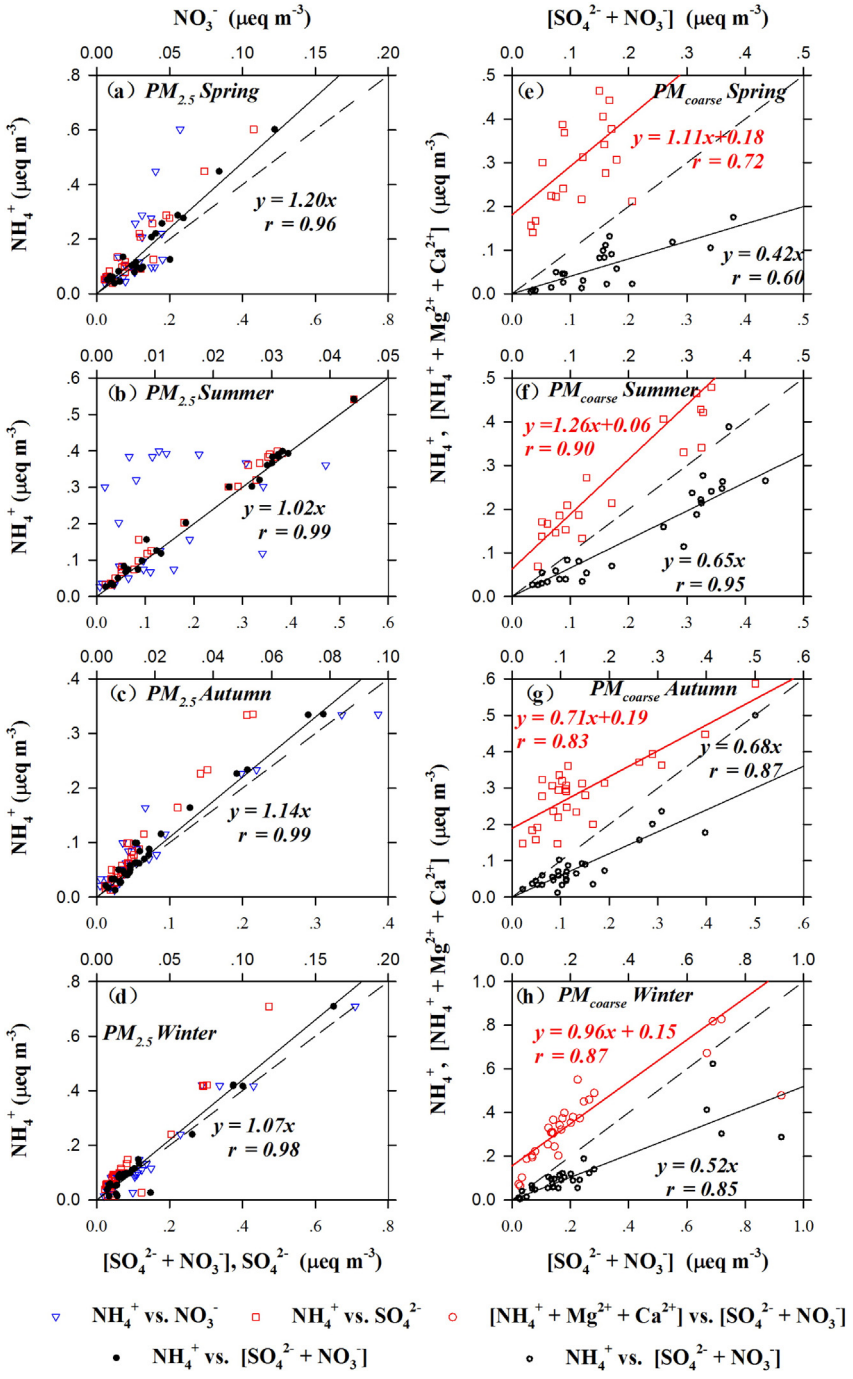

Fig. 5. Scatter plots of NH_4^+ vs. SO_4^{2-}, NH_4^+ vs. NO_3^-, and NH_4^+ vs. $[SO_4^{2-} + NO_3^-]$ in $PM_{2.5}$ in four seasons (a–d), respectively. Scatter plots of NH_4^+ vs. $[SO_4^{2-} + NO_3^-]$ and $[NH_4^+ + Ca^{2+} + Mg^{2+}]$ vs $[SO_4^{2-} + NO_3^-]$ in PM_{coarse} in four seasons (e–h), respectively. Linear regressions between NH_4^+ vs. $[SO_4^{2-} + NO_3^-]$ in $PM_{2.5}$ and PM_{coarse}, and $[NH_4^+ + Ca^{2+} + Mg^{2+}]$ vs. $[SO_4^{2-} + NO_3^-]$ in PM_{coarse} are fitted, along with the 1:1 dashed lines.

vs. $[SO_4^{2-} + NO_3^-]$ in PM_{coarse} were much lower in the range of 0.4–0.7. According to the mass concentrations measured in two sizes, the average ratios of $PM_{2.5}$/TSP for SO_4^{2-}, NO_3^-, and NH_4^+ were 37–53%, 28–36%, and 52–73%, respectively. This meant that SO_4^{2-} and NO_3^- were more favorably formed in larger sizes, and NH_3 was not enough for a full neutralization of the acids in coarse particles. By adding Ca^{2+} and Mg^{2+}, the neutralization of the acids was evidently enhanced, especially in spring and winter with higher correlation coefficients and elevated slopes close to unity (Fig. 5e and 5h). In autumn, the enhanced neutralization of acids was also observed (Fig. 5g), although not as strong as spring and winter. The results above imply that heterogeneous reactions on mineral dust were involved in the formation of SO_4^{2-} and NO_3^- throughout all four seasons over the areas of YL.

On the other hand, the formations of SO_4^{2-} and NO_3^- could have been also significantly influenced by the relative humidity (RH) in spring, autumn, and winter. As shown in Fig. 6 (data in dust event days were excluded), the concentrations of SO_4^{2-} and NO_3^- co-varied consistently due to co-emissions of their precursors with the ambient RH in these three seasons. High yields of SO_4^{2-} and NO_3^- almost all occurred under RH values of higher than 60%, usually in cloudy or foggy days. For instance, sulfate and nitrate in $PM_{2.5}$ (TSP) reached 20.7 (27.6) and 3.5 (11.8) μg m^{-3} on April 17 in 2008 with daily RH of 59%, 5.3–10.2 (16.5–26.9) and 1.0–6.0 (5.8–15.6) μg m^{-3} on October 20–21 in 2008

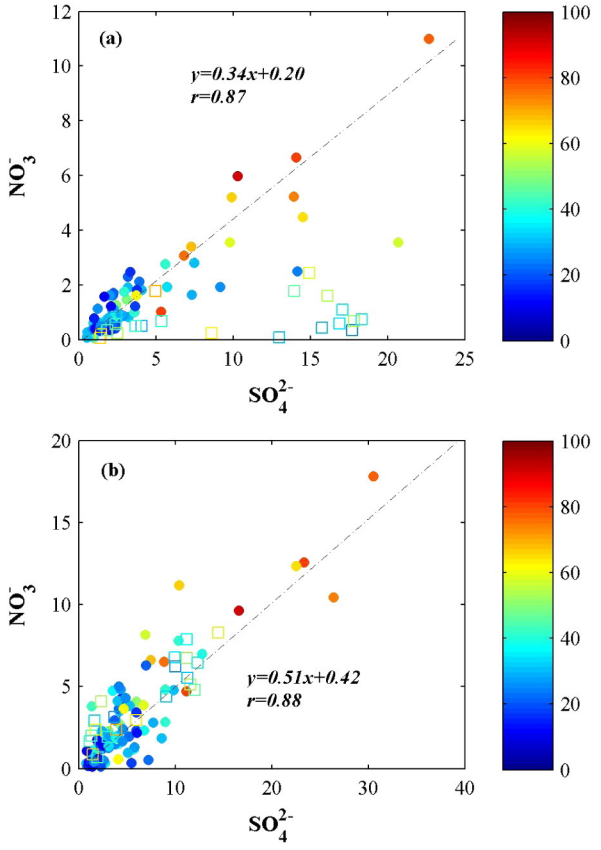

Fig. 6. Relationship between SO_4^{2-} and NO_3^- (μg m^{-3}) in (a) $PM_{2.5}$ and (b) PM_{coarse} (the data of the dust event days on April 1, 2008, and January 21, 2009, were excluded). Square and circle represent the samples collected in summer and in the other seasons, respectively. All the scatters are color coded by their corresponding daily average relative humidity (%).

with daily RH of 81–92%, 6.8–9.9 (14.8–20.3) and 3.1–5.2 (9.6–16.4) μg m^{-3} on November 10–12 in 2008 with daily RH of 66–76%, and 14.0–22.7 (37.1–53.2) and 4.5–11.0 (15.7–28.8) μg m^{-3} on February 3–6 in 2009 with daily RH of 65–80%, respectively. It has been found that heterogeneous reactions between acid gases and pre-existing mineral particles can be promoted in high RH conditions (Zhu et al., 2011), leading to substantial increases of SO_4^{2-} and NO_3^-. In contrast to the poor relationship between SO_4^{2-} and NO_3^- in summer, especially in $PM_{2.5}$ (squares in Fig. 6a), SO_4^{2-} was highly correlated to NO_3^- in spring, autumn, and winter, indicating that SO_4^{2-} and NO_3^- had a similar formation process, i.e., the in-cloud/aqueous process in these three seasons.

3.4. The primary source of sulfate from long-/medium-range transport

Asian dust from the Taklimakan desert in China contains primary sulfate from the paleo-ocean dried sea salts (Huang et al., 2010; Wu et al., 2012), which can be transported far away by dust storms and deposited on the downwind regions. Our observational data in YL showed that particulate SO_4^{2-} substantially increased during the dust event days (Fig. 2d), particularly in PM_{coarse} during those strong dust storm events (Fig. S2c). For instance, SO_4^{2-} in PM_{coarse} increased substantially from 5.6 μg m^{-3} on March 29, 2007, of a non-dust day to 26.6 μg m^{-3} on March 30, 2007, of a dust day. At the same time, element Al in PM_{coarse} climbed from 8.3 μg m^{-3} on March 29 to 72.1 μg m^{-3} on March 30. To further demonstrate the crustal source of SO_4^{2-} over YL, the variations of NO_3^- and black carbon (BC), which had almost no mineral sources, before, during, and after the dust events are also plotted in Figs. 2c and 2e. Opposite to the increase of SO_4^{2-}, the concentrations of BC and NO_3^- significantly decreased in dust event days, which was attributed to the dilution effect by invaded dust. At another observation site (Dunhuang) nearby the dust sources in the northwestern area of China, similar phenomenon was observed that the concentrations of SO_4^{2-} significantly increased in the dust event days but not for NO_3^- (Duvall et al., 2008). These results implied that more SO_4^{2-} could be brought to the YL receptor site along with dust aerosols, either primarily derived from the crustal source or formed by the heterogeneous reaction on the dust surface. The Chinese Loess Plateau, where YL was located, is on the transport pathway and a typical depositional region of the dust plumes from the Taklimakan Desert (Wang et al., 2011; Liu et al., 1994). In this regard, the crustal sulfate over YL could be related to the mineral dust either from the long-range transported dust from the Taklimakan desert or from the local dust emissions re-suspended from the areas around YL.

It should be noted that nitrate did not show any increases as sulfate did during the dust events but actually was significantly reduced in concentration. This phenomenon could be ascribed to two possible reasons. On the one hand, it is already noted that the Taklimakan Desert, which is an upstream source for YL's aerosol was an ocean in the ancient times. SO_4^{2-} is the fourth most abundant ion (mass weight of ~ 7.75%) in seawater and only inferior to Cl^-, Na^+, and Mg^{2+}, while NO_3^- is negligible in seawater with mass weight less than 0.2%. Hence, the transport of the dust from the Taklimakan Desert would not inherently increase the amount of nitrate as it did for sulfate. Recently, a chamber study (He et al., 2014) found that when SO_2 and NOx co-exist with the existence of mineral oxides, both NOx and mineral oxides tended to act as catalysts to promote the conversion of SO_2 to sulfate on the surface of mineral oxides. It is proposed that the catalytic oxidation mechanism of SO_2 on the surface of mineral oxides by NOx is shown as below:

$$SO_2 + 2NO_2 + M \rightarrow M-SO_4 + 2NO \quad (1)$$

$$2NO + O_2 + M \rightarrow 2NO_2 \quad (2)$$

where M represents the surface of mineral oxides. Based on this proposed mechanism, NOx acted more like a catalyst rather than a reactant. Hence, enhanced nitrate is not expected. This chamber result is consistent with Yuan et al. (2008) that the NOR (nitrogen oxidation ratio) was low and even less than 1% during the dust storm of Beijing although it is well known that the NOx level in Beijing was high. Also, it is consistent with this study that NO_3^- decreased during the dust events.

Fig. 7 shows the 3-day backward trajectories starting at YL during the dust event days as highlighted in Fig. 2. It could be clearly visualized that the long-range transported dust that invaded YL was mostly from the direction of W-NW, i.e., from the deserts in western/northwestern China and western/southern Mongolia. The mass ratios of Ca/Al in TSP over YL (~1.0) were much higher than that of ~0.5 from the deserts in middle Inner Mongolia in China or eastern Mongolia (Wang et al., 2011). As a comparison, dust derived from the deserts in western/northwestern China (i.e., Taklimakan Desert) was rich in calcium with a much higher Ca/Al ratio of more than 1.5 (Huang et al., 2010). Hence, the aerosol over YL was likely the result from the mixing of the two major desert source regions with the addition of the local emissions. As observed in the collected dust storm samples, the mass ratio of SO_4^{2-}/3 to the total S in the aerosols over YL was close to 1.00, which meant that almost all of the sulfur in the invaded dust was in the form of soluble SO_4^{2-}. This was contrasted to the dust from the Gobi Desert which had a low SO_4^{2-}/3/S ratio of 0.54 ± 0.09 (Huang et al., 2010). While dust aerosol from the Taklimakan desert was characterized of high fraction of soluble sulfur (SO_4^{2-}/3/S ratio = 0.97 ± 0.12), which was from the paleo-ocean source (Huang et al., 2010). All the evidences above demonstrated that SO_4^{2-} in dust aerosol over YL was significantly impacted by the long-range transported dust from the Taklimakan Desert.

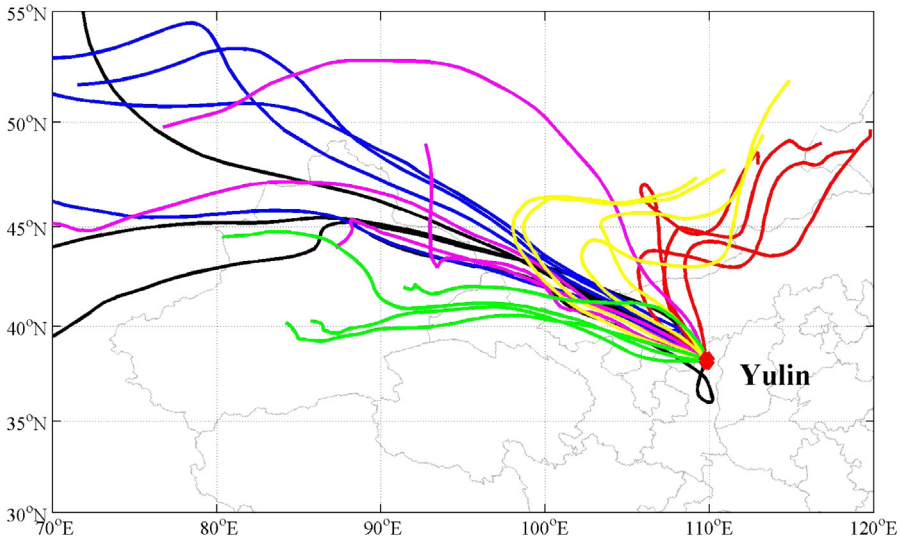

Fig. 7. Seventy-two-hour backward trajectories of the dust event days in spring 2007 and in spring and winter 2008. Black, blue, red, pink, yellow, and green represent the trajectories on March 30, 31 and April 15, 19 in 2007, April 1 in 2008, and January 21 in 2009, respectively. Four trajectories ending at 00, 06, 12, and 18 UTC are computed for each day.

4. Conclusion

Sulfate and nitrate in $PM_{2.5}$ over YL displayed different seasonal variations. The average concentration of SO_4^{2-} in $PM_{2.5}$ was highest in summer, which was probably from the enhanced gas phase oxidation of SO_2. Oppositely, the average concentration of NO_3^- in $PM_{2.5}$ was lowest in summer, attributed to the relatively high ambient temperature that was not favorable for the formation of NH_4NO_3. In comparison, NO_3^- was greatly enhanced in coarse particle in summer as indicated by the highest NO_3^-/PM_{coarse} ratio and the lowest $NO_3^-/PM_{2.5}$ ratio among four seasons. The heterogeneous reaction of SO_2 and NOx on the pre-existing crustal aerosol was responsible for considerable concentrations of coarse mode SO_4^{2-} and NO_3^-, and it was found this formation pathway of secondary inorganic aerosols was ubiquitous throughout all four seasons. In addition to ambient temperature, RH was another important factor that governed the formations of sulfate and nitrate. Different from summer, SO_4^{2-} and NO_3^- in spring, autumn, and winter were more significantly enhanced in those days with relatively high RH values, implicating the important role of in-cloud/aqueous processing in the formations of SO_4^{2-} and NO_3^- in these seasons.

SO_4^{2-} in coarse particles significantly increased in dust event days, while BC and NO_3^- largely decreased. On the one hand, the comparison of the mass ratio of $SO_4^{2-}/3/S$ in the dust aerosols in YL with different dust source regions and the backward trajectory analysis both demonstrated that the long-range transported dust from Taklimakan desert, which was rich in primary sulfate due to its paleo-ocean characteristics, was a major primary source of SO_4^{2-} in YL. On the other hand, heterogeneous reaction of SO_2 on the surface of dust particles has been well known as a major pathway of sulfate formation in the form of $CaSO_4$.

In summer, the regional transport facilitated by the southerlies and southeasterlies contributed to the high secondary aerosol concentrations over YL, while in spring and winter, the prevailing northerlies and northwesterlies promoted chemical interaction between alkaline mineral dust and acid gaseous precursors from local emissions and/or regional emissions on the transport pathway. The transport and deposition of these particles could cause human health issues and alter the regional climate.

Acknowledgment

This work was supported by the National Natural Science Foundation of China (grant nos. 21277030, 41429501 (fund for collaboration with overseas scholars), and 41405115), the Environmental charity project of Ministry of Environmental Protection of China (201409022), the Science and technology development project of Hangzhou (20131813A03 and 20130533B04), and the research project for environmental protection of Hangzhou (2012001). We sincerely thank two anonymous reviewers for improving the quality of this paper.

Appendix A. Supplementary data

Supplementary data to this article can be found online at http://dx.doi.org/10.1016/j.atmosres.2015.09.013.

References

Calvert, J.G., Su, F., 1978. Mechanism of the homogeneous oxidation of sulfur dioxide in the troposphere. Atmos. Environ. 12, 197–226.
Chang, S.C., Chou, C.C.K., Chan, C.C., Lee, C.T., 2010. Temporal characteristics from continuous measurements of PM2.5 and speciation at the Taipei Aerosol Supersite from 2002 to 2008. Atmos. Environ. 44, 1088–1096.
Duvall, R.M., Majestic, B.J., Shafer, M.M., Chuang, P.Y., Simoneit, B.R.T., Schauer, J.J., 2008. The water-soluble fraction of carbon, sulfur, and crustal elements in Asian aerosols and Asian soils. Atmos. Environ. 42, 5872–5884.
Fu, Q.Y., Zhuang, G.S., Wang, J., Xu, C., Huang, K., Li, J., Hou, B., Lu, T., Streets, D.G., 2008. Mechanism of formation of the heaviest pollution episode ever recorded in the Yangtze River Delta, China. Atmos. Environ. 42, 2023–2036.
Guinot, B., Cachier, H., Sciare, J., Tong, Y., Xin, W., Jianhua, Y., 2007. Beijing aerosol: Atmospheric interactions and new trends. J. Geophys. Res.-Atmos. 112, D14314. http://dx.doi.org/10.1029/2006JD008195.
Guo, Z.B., Li, Z.Q., Farquhar, J., Kaufman, A.J., Wu, N.P., Li, C., Dickerson, R.R., Wang, P.C., 2010a. Identification of sources and formation processes of atmospheric sulfate by sulfur isotope and scanning electron microscope measurements. Journal of Geophysical Research-Atmospheres 115, D00K07. http://dx.doi.org/10.1029/2009JD012893.
Guo, S., Hu, M., Wang, Z.B., Slanina, J., Zhao, Y.L., 2010b. Size-resolved aerosol water-soluble ionic compositions in the summer of Beijing: implication of regional secondary formation. Atmos. Chem. Phys. 10, 947–959.
He, H., Wang, Y.S., Ma, Q.X., Ma, J.Z., Chu, B.W., Ji, D.S., Tang, G.Q., Liu, C., Zhang, H.X., Hao, J.M., 2014. Mineral dust and NOx promote the conversion of SO_2 to sulfate in heavy pollution days. Sci. Rep. 4. http://dx.doi.org/10.1038/srep04172.
Huang, K., Zhuang, G., Li, J., Wang, Q.Z., Sun, Y., Lin, Y., Fu, J.S., 2010. Mixing of Asian dust with pollution aerosol and the transformation of aerosol components during the dust storm over China in spring 2007. J. Geophys. Res. 115, D00K13. http://dx.doi.org/10.1029/2009JD013145.
IPCC, 2007. The Physical Science Basis, Contributino of Working Group I to the Fourth Assessment Report of the Intergovernmental Panel on Climate Change. Cambridge University Press, New York, USA.
Kong, L., Yang, Y.W., Zhang, S.Q., Zhao, X., Du, H.H., Fu, H.B., Zhang, S.C., Cheng, T.T., Yang, X., Chen, J.M., Du, D., Shen, J.D., Hong, S.M., Jiao, L., 2014. Observations of linear dependence between sulfate and nitrate in atmospheric particles. J. Geophys. Res.-Atmos. 119, 341–361. http://dx.doi.org/10.1002/2013JD020222.
Li, L., Chen, Z.M., Zhang, Y.H., Zhu, T., Li, J.L., Ding, J., 2006. Kinetics and mechanism of heterogeneous oxidation of sulfur dioxide by ozone on surface of calcium carbonate. Atmos. Chem. Phys. 6, 2453–2464.
Lida, D.R., 2006. Handbook of Chemistry and Physics: A Ready-Reference Book of Chemical and Physical Data. 86th ed. CRC Press, New York 14–17.

Lin, Y., Huang, K., Zhuang, G., Fu, J.S., Wang, Q., Liu, T., Deng, C., Fu, Q., 2014. A multi-year evolution of aerosol chemistry impacting visibility and haze formation over an Eastern Asia megacity, Shanghai. Atmos. Environ. 92, 76–86.
Liu, C.Q., Masuda, A., Okada, A., Yabuki, S., Fan, Z.L., 1994. Isotope geochemistry of quaternary deposits from the arid lands in Northern China. Earth Planet. Sci. Lett. 127, 25–38.
Lu, Z., Streets, D.G., Zhang, Q., Wang, S., Carmichael, G.R., Cheng, Y.F., Wei, C., Chin, M., Diehl, T., Tan, Q., 2010. Sulfur dioxide emissions in China and sulfur trends in East Asia since 2000. Atmos. Chem. Phys. 10, 6311–6331.
Malm, W.C., Sisler, J.F., Huffman, D., Eldred, R.A., Cahill, T.A., 1994. Spatial and seasonal trends in particle concentration and optical extinction in the United-States. J. Geophys. Res.-Atmos. 99, 1347–1370.
Manktelow, P.T., Carslaw, K.S., Mann, G.W., Spracklen, D.V., 2010. The impact of dust on sulfate aerosol, CN and CCN during an East Asian dust storm. Atmos. Chem. Phys. 10, 365–382.
Morino, Y., Ohara, T., Kurokawa, J., Kuribayashi, M., Uno, I., Hara, H., 2011. Temporal variations of nitrogen wet deposition across Japan from 1989 to 2008. J. Geophys. Res.-Atmos. 116, D06307. http://dx.doi.org/10.1029/2010JD015205.
Pathak, R.K., Wu, W.S., Wang, T., 2009. Summertime PM2.5 ionic species in four major cities of China: nitrate formation in an ammonia-deficient atmosphere. Atmos. Chem. Phys. 9, 1711–1722.
Seinfeld, J.H., Pandis, S.N., 2006. Atmospheric Chemistry and Physics: From air Pollution to Climate Change. 2nd ed. New York, USA, John Wiley & Sons.
Shaanxi Provincial Environmental Protection Department, 2007–2009. Environment condition periodic reports of Shaanxi Province (http://www.snepb.gov.cn/admin/pub_newschannel.asp?Page = 2&chid = 100271 (in Chinese)).
Shi, Z., Zhang, D., Hayashi, M., Ogata, H., Ji, H., Fujiie, W., 2008. Influences of sulfate and nitrate on the hygroscopic behaviour of coarse dust particles. Atmos. Environ. 42, 822–827.
Sipila, M., Berndt, T., Petaja, T., Brus, D., Vanhanen, J., Stratmann, F., Patokoski, J., Mauldin, R.L., Hyvarinen, A.P., Lihavainen, H., Kulmala, M., 2010. The role of sulfuric acid in atmospheric nucleation. Science 327, 1243–1246.
Sun, J.M., Zhang, M.Y., Liu, T.S., 2001. Spatial and temporal characteristics of dust storms in China and its surrounding regions, 1960–1999: relations to source area and climate. J. Geophys. Res.-Atmos. 106, 10325–10333.
Streets, D.G., Bond, T.C., Carmichael, G.R., Fernandes, S.D., Fu, Q., He, D., Klimont, Z., Nelson, S.M., Tsai, N.Y., Wang, M.Q., Woo, J.H., Yarber, K.F., 2003. An inventory of gaseous and primary aerosol emissions in Asia in the year 2000. J. Geophys. Res.-Atmos. 108 (D21), 8809. http://dx.doi.org/10.1029/2002JD003093.
Streets, D.G., Waldhoff, S.T., 2000. Present and future emissions of air pollutants in China: SO2, NOx, and CO. Atmos. Environ. 34, 363–374.
Takahashi, Y., Miyoshi, T., Yabuki, S., Inada, Y., Shimizu, H., 2008. Observation of transformation of calcite to gypsum in mineral aerosols by CaK-edge X-ray absorption near-edge structure (XANES). Atmos. Environ. 42, 6535–6541.
Usher, C.R., Al-Hosney, H., Carlos-Cuellar, S., Grassian, V.H., 2002. A laboratory study of the heterogeneous uptake and oxidation of sulfur dioxide on mineral dust particles. J. Geophys. Res.-Atmos. 107 (D23), 4713. http://dx.doi.org/10.1029/2002JD002051.
Wu, F., Zhang, D.Z., Cao, J.J., Xu, H.M., An, Z.S., 2012. Soil-derived sulfate in atmospheric dust particles at Taklimakan desert. Geophys. Res. Lett. 39, L24803. http://dx.doi.org/10.1029/2012GL054406.
Wang, Q.Z., Zhuang, G.S., Li, J.A., Huang, K., Zhang, R., Jiang, Y.L., Lin, Y.F., Fu, J.S., 2011. Mixing of dust with pollution on the transport path of Asian dust—revealed from the aerosol over Yulin, the north edge of Loess Plateau. Sci. Total Environ. 409, 573–581.
Wang, Y., Zhuang, G.S., Zhang, X.Y., Huang, K., Xu, C., Tang, A.H., Chen, J.M., An, Z.S., 2006. The ion chemistry, seasonal cycle, and sources of PM2.5 and TSP aerosol in Shanghai. Atmos. Environ. 40, 2935–2952.
Xiao, R., Takegawa, N., Kondo, Y., Miyazaki, Y., Miyakawa, T., Hu, M., Shao, M., Zeng, L.M., Hofzumahaus, A., Holland, F., Lu, K., Sugimoto, N., Zhao, Y., Zhang, Y.H., 2009. Formation of submicron sulfate and organic aerosols in the outflow from the urban region of the Pearl River Delta in China. Atmos. Environ. 43, 3754–3763.
Yao, X., Chan, C.K., Fang, M., Cadle, S., Chan, T., Mulawa, P., He, K., Ye, B., 2002. The water-soluble ionic composition of PM2.5 in Shanghai and Beijing, China. Atmos. Environ. 36, 4223–4234.
Yuan, H., Wang, Y., Zhuang, G., 2003. The simultaneous determination of organic acid, MSA with inorganic anions in aerosol and rainwater by ion chromatography (in Chinese). J. Instrum. Anal. 6, 6–12.
Yuan, H., Zhuang, G.S., Li, J., Wang, Z.F., Li, J., 2008. Mixing of mineral with pollution aerosols in dust season in Beijing: revealed by source apportionment study. Atmos. Environ. 42, 2141–2157.
Yue, D.L., Hu, M., Zhang, R.Y., Wang, Z.B., Zheng, J., Wu, Z.J., Wiedensohler, A., He, L.Y., Huang, X.F., Zhu, T., 2010. The roles of sulfuric acid in new particle formation and growth in the mega-city of Beijing. Atmos. Chem. Phys. 10, 4953–4960.
Zhang, B., Tsunekawa, A., Tsubo, M., 2008. Contributions of sandy lands and stony deserts to long-distance dust emission in China and Mongolia during 2000–2006. Glob. Planet. Chang. 60, 487–504.
Zhang, D.Z., Shi, G.Y., Iwasaka, Y., Hu, M., 2000. Mixture of sulfate and nitrate in coastal atmospheric aerosols: individual particle studies in Qingdao (36 degrees 04′ N, 120 degrees 21′ E), China. Atmos. Environ. 34, 2669–2679.
Zhang, Q., Streets, D.G., Carmichael, G.R., He, K.B., Huo, H., Kannari, A., Klimont, Z., Park, I.S., Reddy, S., Fu, J.S., Chen, D., Duan, L., Lei, Y., Wang, L.T., Yao, Z.L., 2009. Asian emissions in 2006 for the NASA INTEX-B mission. Atmos. Chem. Phys. 9, 5131–5153.
Zhang, Q., Streets, D.G., He, K., Wang, Y., Richter, A., Burrows, J.P., Uno, I., Jang, C.J., Chen, D., Yao, Z., Lei, Y., 2007. NOx emission trends for China, 1995–2004: the view from the ground and the view from space. J. Geophys. Res.-Atmos. 112, D22306. http://dx.doi.org/10.1029/2007JD008684.
Zhang, T., Cao, J.J., Tie, X.X., Shen, Z.X., Liu, S.X., Ding, H., Han, Y.M., Wang, G.H., Ho, K.F., Qiang, J., Li, W.T., 2011. Water-soluble ions in atmospheric aerosols measured in Xi'an, China: seasonal variations and sources. Atmos. Res. 102, 110–119.
Zhao, J.P., Zhang, F.W., Xu, Y., Chen, J.S., Yin, L.Q., Shang, X.S., Xu, L.L., 2011. Chemical characteristics of particulate matter during a heavy dust episode in a coastal city, Xiamen, 2010. Aerosol Air Qual. Res. 11, 300–309.
Zhu, T., Shang, J., Zhao, D.F., 2011. The roles of heterogeneous chemical processes in the formation of an air pollution complex and gray haze. Sci. China: Chem. 54, 145–153.
Zhuang, G.S., Guo, J.H., Yuan, H., Zhao, X.J., 2001. The compositions, sources, and size distribution of the dust storm from China in spring of 2000 and its impact on the global environment. Chin. Sci. Bull. 46, 895–901.